Raman scattering and phase transitions of V_2O_3†

N. Kuroda* and H. Y. Fan
Department of Physics, Purdue University, West Lafayette, Indiana 47907
(Received 3 August 1977)

Raman scattering in single crystals of V_2O_3 has been studied in the range from ~20 K to room temperature. Metal to insulator, crystallographic, and antiferromagnetic-ordering transitions take place concurrently at $T_t \sim 150$ K. The observed spectra showed a drastic change at T_t. On either side of T_t, peaks were observed which had intensities rather insensitive to the variation of temperature. These peaks are identifiable as phonon excitations, and the peaks of the two temperature regions can be correlated on the basis of the structural transition of the crystal. One peak was observed in the low-temperature region, the intensity of which decreased strongly with increasing temperature, becoming unobservable at $T \gtrsim T_t$. Clearly, this peak involved the excitation of magnons which resulted from the magnetic transition.

I. INTRODUCTION

Phase transition is a subject of great interest in physics, and V_2O_3 is one of the crystals in which three kinds of transitions take place concurrently. As the temperature is lowered under normal pressure, the electrical resistivity of the crystal undergoes a metal-insulator transition at $T_t \sim 150$ K. Simultaneously, the crystallographic structure makes a α-corundum–monoclinic transition, and the crystal becomes antiferromagnetic. Numerous studies of various properties have been made, and theoretical treatments using different approaches have been attempted.[1] A conclusive thorough understanding has yet to be established.

Studies of Raman scattering yield information on certain crystal excitations. The scattering associated with phonon excitation can be effective for the study of crystallographic transition, and magnon scattering, if observed, can be significant for the study of magnetic ordering and magnetic transition. Little information is available on phonons in V_2O_3. Three peaks at $\nu = 500$, 750, and 820 cm^{-1} with some associated fine structures were observed in the infrared absorption spectrum of 77 K, and some fluctuation corresponding to the peaks could be discerned in the spectrum for 293 K.[2] The peaks were attributed to the excitation of infrared-active phonons. It will be pointed out that such phonons are not expected to be active in Raman scattering. In a study of phonon scattering in TiO_3,[3] it was mentioned in passing that a Raman spectrum was observed on V_2O_3 at 300 K, with the most intense mode being A_{1g} at 240 cm^{-1}. We report in this paper studies of Raman scattering in a range from ~20 K to room temperature. Changes of phonon scattering due to the structural transition, and magnon scattering brought out by the transition to antiferromagnetic state have been observed.

II. THEORY

The α-corundum crystallographic structure of V_2O_3 has the symmetry of the $R\bar{3}c$ space group[4] with the D_{3d} point group. Shown in Fig. 1(a) are the hexagonal unit cell and the inscribed trigonal primitive cell[5]; only the V ions are indicated. The c/a ratio of the hexagonal unit cell is ~2.827 at room temperature. There are two units of V_2O_3 in the primitive cell and four units of V_2O_3 in the unit cell. Some symmetry elements of the point group are indicated: the three-

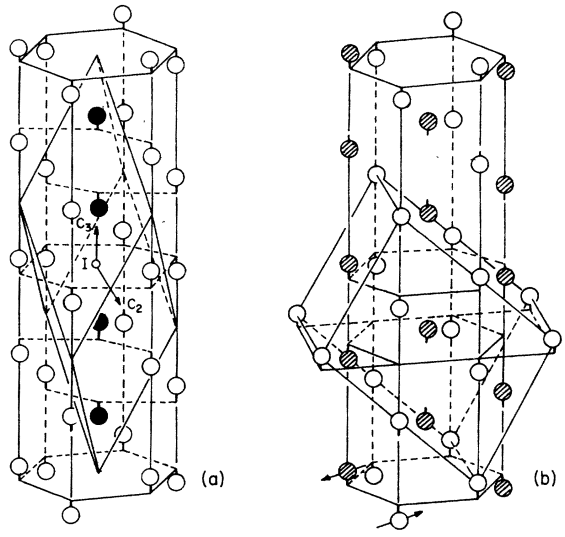

FIG. 1. (a) Hexagonal unit cell with inscribed trigonal primitive cell of V_2O_3 in the α-corundum phase; V ions are shown. Some elements, C_3, C_2, and I, of the point group are shown. (b) Hexagonal unit cell of the α-corundum phase and primitive cell of the monoclinic phase; hatched and open circles represent ions of opposite spins.

fold rotation axis C_3, one of the three twofold rotation axes C_2, and the inversion center I. Figure 1(b) serves to indicate the effect of structure distortion which occurs at the phase transition.[5] Shown are the original hexagonal unit cell and a cell which leads to the monoclinic primitive cell of the distorted structure. The space group of the crystal changes to $B2/b$,[4] with the point group C_{2h}. The origin of the C_{2h} group is located at a V ion, and the twofold rotation axis of the group is parallel to the C_2 axis shown in Fig. 1(a).

At $T \geq T_t$, the point group D_{3d} has six irreducible representations: A_{1g}, A_{1u}, A_2, A_{2u}, E_g, E_u. There are two units of V_2O_3 in a primitive lattice cell hence three are 30 branches of normal modes. The point-group representations of the $k=0$ modes have been shown to be[6]

$$2A_{1g}+2A_{1u}+3A_{2u}+5E_g+5E_u \ . \tag{1}$$

One of the acoustical modes which corresponds to a translation along the C_3 axis has an A_{2u} representation. The other two acoustical modes corresponding to translations perpendicular to this axis have the E_u representation. The group D_{3d} has an inversion element. The subscript g or u of a representation indicates that the mode is symmetrical or antisymmetrical with respect to inversion. Only the g modes may be Raman active, and only the u modes may be active for infrared absorption. Since g modes are not accompanied by a long-range electric field, there are no such complications as splitting of degeneracy and variation of frequency shift with variation of light beams relative to each other or relative to the crystal orientation. Consideration of the characters of representation shows that A_{1g} and E_g are Raman active while A_{2g} is not. Thus, seven Raman lines may be expected for the crystal, two lines associated with A_{1g} modes and five lines associated with E_g modes.

At $T \leq T_t$, the space group changes to $B2/b$. The point group C_{2h} of the distorted structure is a subgroup of D_{3d} of the α-corundum structure. The group C_{2h} contains also the inversion, and it has four irreducible representations: A_g, A_u, B_g, B_u. The translational acoustical modes have A_u and B_u representations. A_g and B_g modes are Raman active. The correlation between the representations of D_{3d} and those of its subgroup C_{2h} is[7]

$$\frac{A_{1g}\quad A_{2g}\quad A_{1u}\quad A_{2u}\quad E_g\quad E_u}{A_g\quad B_g\quad A_u\quad B_u\quad A_g+B_g\quad A_u+B_u} \ . \tag{2}$$

With the distortion, an A_{1g} Raman line, i.e., a Raman line involving phonons of A_{1g} representation, leads to an A_g line, and an E_g line leads to a pair of A_g and B_g lines. In addition, a B_g line evolves from each of the three inactives A_{2g} modes.

Raman scattering depends on the polarizability tensor α characteristic of the phonon involved. The non-vanishing components of α are indicated below for the phonon species of the two crystal structures[8]:

$$D_{3d}: \quad \begin{matrix} A_{1g} \\ \begin{vmatrix} a & & \\ & a & \\ & & b \end{vmatrix} \end{matrix}, \quad \begin{matrix} E_g' \\ \begin{vmatrix} c & & \\ & -c & d \\ & d & \end{vmatrix} \end{matrix}, \quad \begin{matrix} E_g'' \\ \begin{vmatrix} -c & & \\ & -c & -d \\ & -d & \end{vmatrix} \end{matrix}; \tag{3}$$

$$C_{2h}: \quad \begin{matrix} A_g \\ \begin{vmatrix} a & & d \\ & b & \\ d & & c \end{vmatrix} \end{matrix}, \quad \begin{matrix} B_g \\ \begin{vmatrix} & e & \\ e & & f \\ & f & \end{vmatrix} \end{matrix} . \tag{4}$$

The two tensors for the E_g species of D_{3d} are differentiated by superscripts. The tensors for the trigonal group D_{3d} refer to a coordinate system with $\vec{z}$ parallel to a C_3, and $\vec{x}$ parallel to a $\vec{C}_2$. The tensors of C_{2h} refer to a coordinate system with $\vec{y} \| \vec{C}_2$. The intensity I of a Raman line is given by

$$I \propto |\hat{e}_i \alpha \hat{e}_s|^2 \ , \tag{5}$$

where $\hat{e}$ is a unit vector giving the polarization of radiation, and the subscripts i and s indicate, respectively, the incident and the scattered radiations. The intensity of a Raman line varies with the polarization directions of the incident and the scattered radiations, according to the relative magnitudes of the tensor components for the phonons involved.

We have discussed phonons in the antiferromagnetic phase in terms of the Fedorov space group $B2/b$ and the classical point group C_{2h} of the structure, assuming the magnetic effects on phonon symmetry to be small. In regards to magnon excitations, however it is necessary to consider the magnetic groups. It has been found[9] that, in the antiferromagnetic phase, the magnetic moments are ferromagnetically aligned in layers of V ions perpendicular to a hexagonal a axis, with a reversal between adjacent layers. The ordered moment of $1.2\mu_B$ per V atom is oriented perpendicular to the hexagonal a axis at an angle of 71° from the hexagonal c axis. In Fig. 1(b), open and filled circles are used to differentiate V ions associated with the two opposite moments. Of the four elements E, C_2, I, σ_h of the ordinary point group C_{2h}, the operations C_2 and I exchange V ions of opposite moments. The magnetic point group[10] is $2'/m$ consisting of a unitary subgroup C_{1h} with elements E and σ_h, and antiunitary elements RI and RC_2. Single-valued representations are pertinent for magnon transitions. C_{1h} has two single-valued irreducible representations A' and A'' which correspond to two corepresentations DA' and DA'' of the magnetic point group. It has been shown[11] that the important mechanism of magnon scattering is the electric-dipole coupling of the photon to the magnetic system, by virtue of spin-orbit coupling. On this basis, the magnon scattering is determined by a Raman tensor R, according to an expression similar to (5). The tensor has the following

forms for states of the two corepresentations[12]:

$$(DA')\begin{vmatrix} A & B & 0 \\ D & E & 0 \\ 0 & 0 & I \end{vmatrix}\ ;\ (DA'')\begin{vmatrix} 0 & 0 & 0 \\ 0 & 0 & F \\ G & H & 0 \end{vmatrix}\ . \qquad (6)$$

III. EXPERIMENTAL RESULTS AND DISCUSSION

Measurements were made by using an argon-ion cw laser, Corad Model 54, as the source. The absorption of V_2O_3 at the laser wavelength of 5145 or 4880 Å is very high, making it necessary to measure scattering in reflection. A polarizer was inserted in the laser beam, giving polarization in the plane of incidence. The beam was incident on sample surface at the Brewster angle $\theta = 60.4°$ in order to minimize the reflected radiation with polarization in the plane of incidence. The scattered radiation in the plane of incidence was collected at 90° from the laser beam. After passing through an analyzer, the collected radiation was dispersed by a Spex 31402 double monochromator and detected by a photon-counting system with a *S*-20 photomultiplier. The sample was mounted in a Janis Model 8 optical Dewar. V_2O_3 crystals tend to crack upon cooling or warming through the transition temperature, on account of the first-order structural change. Therefore, it was necessary to use very thin samples for our measurements. Thin slabs were cut from the crystals grown at Purdue, and they were polished to a thickness of 10–20 μm. The problem of sample cracking was found to be aggravated by the measurements made. It was desirable to use a laser intensity as high as possible in order to obtain a high scattering intensity for measurement. In so doing, a small volume of the sample under the laser beam could be at a significantly higher temperature than the rest of the sample. The situation is especially serious in regard to cracking when the bulk of the sample is close to the transition temperature. The temperature of the sample was indicated by a GaAs thermosensor. If needed, a better estimate of the temperature at which the scattering effectively occurred was obtained from the intensity ratio of Stokes and anti-Stokes scatterings.

Figure 2 shows the result of our measurements for the α-corundum phase of V_2O_3. Shown are the results obtained on two samples. The surface of each sample contained the two directions $\hat{I}$ and $\hat{II}$ which are normal to the (101) and ($\bar{1}$20) hexagonal planes, respectively. In terms of the right-handed Cartesian coordinates $\vec{x} \| \vec{C}_2$ and $\vec{z} \| \vec{C}_3$,

$$\hat{I} = \frac{(1,\ \tan 30°,\ a/c)}{[1+\tan^2 30° + (a/c)^2]^{1/2}}$$

$$= (0.829,\ 0.479,\ 0.293)\ ,$$

$$\hat{II} = \frac{(1,\ (2-\sin 30°)/\cos 30°,\ 0))}{[1+(2-\sin 30°)^2/\cos^2 30°]^2}$$

$$= (-0.500,\ -0.865,\ 0)\ ,$$

where $a/c \approx 1/2.2827$ is the ratio of hexagonal axes of V_2O_3 at $T \lesssim 300$K. The measurements on sample 302-2-2 were made with $\hat{II}$ in the plane of incidence. The angle θ of incidence being the Brewster angle, the laser beam inside the sample had a component $E_i \cos(\frac{1}{2}\pi - \theta)$ parallel to $\hat{II}$ and a component $E_i \cos\theta$ normal to the sample surface. We denote this direction of $\vec{E}_i$ by $\hat{II}_1$. The measurements on sample 302-2-4 were made with $\hat{I}$ in the plane of incidence. Similarly, the direction of $\vec{E}_i$ for this case will be denoted by $\hat{I}_1$. Depending on the setting of the analyzer in the scattered beam, the radiation measured was scattered with electric field $\vec{E}_s \| \hat{I}$ or $\vec{E}_s \| \hat{II}_1$ in sample 302-2-2 and with $\vec{E}_s \| \hat{II}$ or $\vec{E}_s \| \hat{I}_1$ in sample 302-2-4. It is easily shown that

$$\hat{I}_1 = (0.584,\ 0.338,\ 0.728)\ ,$$

$$\hat{II}_1 = (-0.566,\ 0.672,\ 0.475)\ .$$

In terms of the polarization $\vec{E}_i$ of the exciting radiation and the polarization $\vec{E}_s$ of the measured scattering, the results obtained on sample 302-2-2 were II_1II_1 and II_1I, and the results obtained on sample 302-2-4 were I_1I_1 and I_1II.

The frequency shift and the dependence of intensity of polarizations are listed in the first four columns of Table I, for the five observed scattering peaks. Information in the fourth column is given in parentheses. It is less accurate since the information depends on the correlation of separate measurements which were made on different samples. The variation of intensity with polarizations can be theoretically calculated according to (5) by using each of the three tensors listed

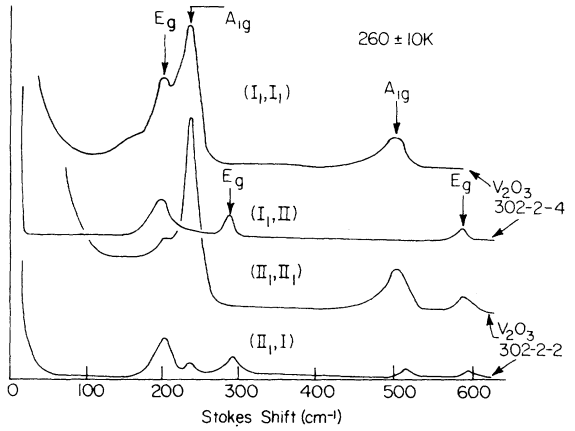

FIG. 2. Spectra of scattering for different polarizations, at a $T > T_t$.

TABLE I. Identification of the scattering peaks observed in the spectra shown in Fig. 3. The frequency shift of peaks are given in column 1. The columns under "Experimental observation" give the observed comparison of intensities for different polarizations. The remianing columns under "Theoretical fit" give the assigned phonon mode, the components of the α tensor used in calculation, and the calculated intensity ratios.

	Experimental observation				Theoretical fit	
Frequency	Sample			Phonon mode	Components	Intensity ratios
shift (cm^{-1})	302-2-4 I_1I_1/I_1II	302-2-4 II_1II_1/II_1I				$I_1I_1 : I_1II : II_1II_1 : II_1I$
203	$\lesssim 1$	$<<1$	$(I_1II - II_1I)$	E_g'	$d = \frac{1}{5}c$	0.2 : 0.4 : ~0 : 1
231	$>>1$	$>>1$	$(I_1I_1 - II_1II_1)$	A_{1g}	$a = b$	1 : ~0 : 1 : ~0
290	0	0	$(I_1II - II_1I)$	E_g'	$\lvert d\rvert << \lvert c\rvert$	0.1 : 0.6 : ~0 : 1
500	$>>1$	$>>1$	$(I_1I_1 - II_1II_1)$	A_{1g}	$a = b$	1 : ~0 : 1 : ~0
590	$<<1$	$\gtrsim 1$	$(I_1II - II_1II_1)$	E_g'	$c = -\frac{1}{2}d$	0.25 : 1 : 0.7 : 0.7

in (3). The phonon mode involved in each scattering peak is identified by fitting the observed with the calculated polarization dependence of intensity. The identified modes are listed in the fifth column. The sixth column gives the ratio of the tensor components which gives the calculated polarization dependence listed in the last column. Comparison of the last column with the experimental results shows that the fitting is satisfactory. We note that a reasonable fitting for each scattering peak cannot be obtained by attributing the peak to a different phonon mode.

The scattering was found to make an abrupt change as the temperature was lowered. The measured spectra for the samples at a temperature below T_t are shown in Fig. 3. According to the structural transformation discussed in connection with Fig. 1, the spectra refer to

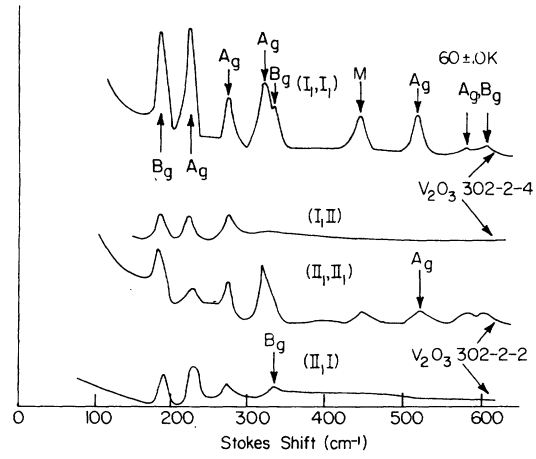

FIG. 3. Spectra of scattering for different polarizations, at a $T < T_t$.

$$\vec{E}_s \| \hat{1}_1 = (0.338,\ -0.584,\ 0.728),$$
$$\hat{2}_1 = (0.672,\ 0.566,\ 0.475)\ .$$

and

$$\vec{E}_i \| \hat{1}_1, \hat{2}_1, \hat{1} = (0.479,\ -0.829,\ 0.293),$$
$$\hat{2} = (0.865,\ 0.500,\ 0)\ ,$$

in terms of right-handed Cartesian coordinates with $\vec{y} \| \vec{C}_2$. The results obtained from sample 302-2-2 are 2_12_1 and 2_11, and those measured on sample 302-2-4 are 1_11_1 and 1_12.

The frequency shift as a function of temperature is given in Fig. 4 for the various scattering peaks. The dashed lines indicate the association of the peaks in the monoclinic phase with the peaks in the α-corundum phase, according to the correlation given by (2). As shown in (4), the α-tensor for the phonon species A_g contains four different nonvanishing components and that of B_g has only two. It is more meaningful to assess whether the polarization dependence of a peak is consistent with B_g, whereas the matching with A_g is too flexible. For a pair of peaks associated with the lowest E_g at ~203 cm^{-1}, only the polarization dependence of the lower one can be fitted by B_g; the intensities

$$1_11_1 : 1_12 : 2_12_1 : 2_11 = 1 : 02 : 1 : 03$$

calculated with $e/f = 4$ give a reasonable fit. The next higher E_g at ~290 cm^{-1} is not clearly split to warrant quantitative analysis; however, the component of higher frequency shift rather than the component prominant in 1_11_1 and 2_12_1 is qualitatively consistent with B_g. The two peaks associated the E_g at ~590 cm^{-1} are very weak, and it is not possible to assign them between B_g and A_g.

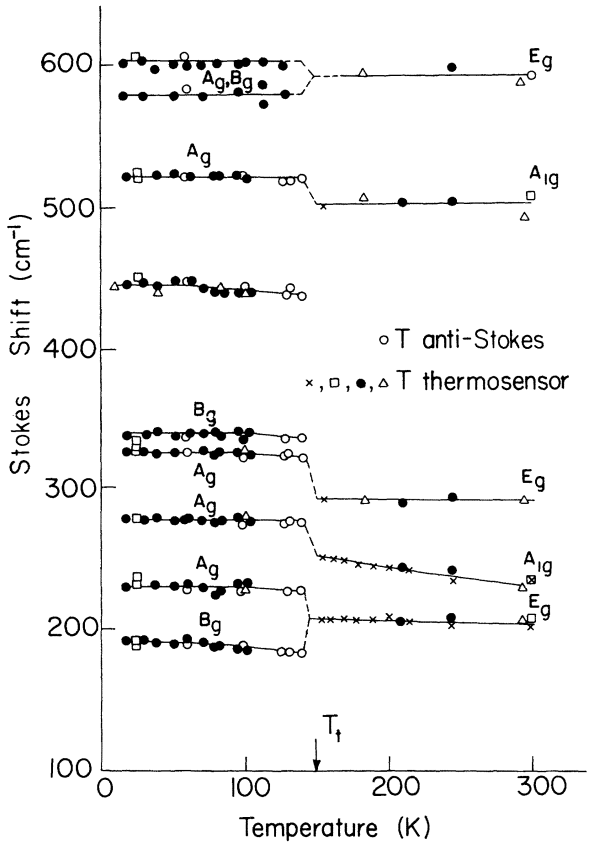

FIG. 4. Frequency shift as function of T_t for the various scattering peaks. Correlation of peaks of the two phases are shown by dashed lines.

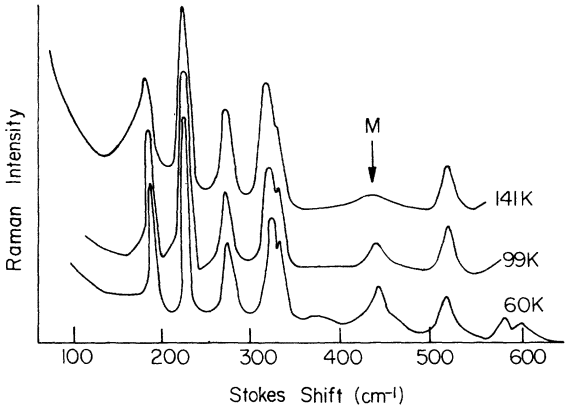

FIG. 5. Spectra of scattering for three different temperatures below T_t.

The peak denoted M in Fig. 3 is of special interest. It is not related to phonon scattering of the α-corundum phase. More importantly, its intensity increases markedly with decreasing temperature in contrast to the intensities of phonon peaks which are largely insensitive to temperature. The observation is illustrated by the spectra shown in Fig. 5 for three different temperatures. The temperature dependence of M peak plotted in Fig. 6 shows the peak to beome unobservable as the transition temperature T_t was reached. Clearly, the peak represents a magnon scattering. The measurements made indicate the dependence of intensity on polarization to be

$$1_11_1 : 1_12 : 2_12_1 : 2_11 \sim 1 : << 1 : \tfrac{1}{3} : << 1 \ .$$

The result is insufficient for ascertaining the symmetry species of the magnon since each of the two tensors in (6) involves as many as four nonvanishing components. Detailed investigation is needed in order to fully exploit the magnon scattering for information on the magnetiic state. Attempts were made to determine the effect of a strong applied dc magnetic field on the three types of transitions. Electrical measurements showed that a magnetic field up to 100 kG did not significantly affect the M-I transition. Measurements of scattering at $T < T_t$ have not yet been made due to the difficulty of cooling the sample sufficiently since a sample mounted inside the superconducting solenoid is not conveniently cooled by the liquid-He vapor.

Measurements of Raman scattering coupled with the measurement of electrical resistance provide a simple method of ascertaining the concurrence of the different transitions under various conditions. Such information should be important for understanding the interrelationship of the transitions.

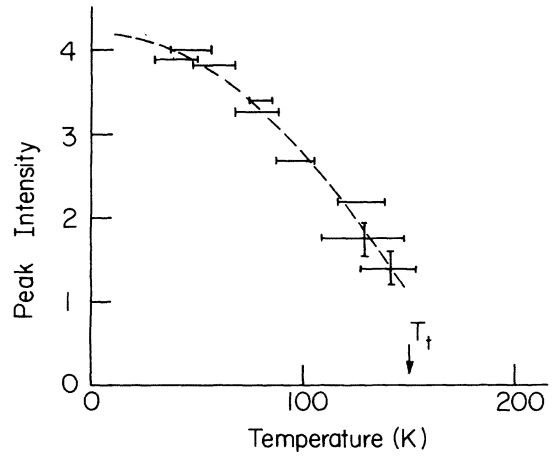

FIG. 6. Peak intensity of the M peak as a function of T.

†Work supported in part by NSF Grant No. DMR 75-1118 and by the NSF MRL Program No. DMR 72-03018A04.

*On leave from Tohoku University, Japan. Present address: Research Institute for Iron, Steel and Other Metals, Tohoku University, Sendai, Japan.

[1]For a review of publications, see J. M. Honig and L. L. Van Zandt, Ann. Rev. Mater. Sci. 5, 225 (1975).

[2]M. S. Kozyreva, V. N. Novikov, and B. A. Tallerchik, Fiz. Tverd. Tela 14, 749 (1972) [Sov. Phys.-Solid State 14, 639 (1972)].

[3]A. M. Mooradian and P. M. Raccah, Phys. Rev. B 3, 4253 (1971).

[4]D. B. McWhan and J. P. Remeika, Phys. Rev. B 2, 3734 (1970); P. D. Dernier and M. Marezio, *ibid.* 2, 3771 (1970).

[5]J. B. Goodenough, in *Proceedings of the Tenth International Conference on the Physics of Semiconductors, Cambridge, Massachusettes* (National Technical Information Service, Natl. Bur. Stand., U. S. Department of Commerce, Washington, D. C., 1970), p. 304.

[6]S. Bhagavantam and T. Venkatarayudu, Proc. Indian Acad. Sci. A 9, 224 (1939).

[7]E. B. Wilson, Jr., J. C. Decius, and P. C. Cross, *Molecular Vibrations, The Theory of Infrared and Raman Vibrational Spectra* (McGraw-Hill, New York, 1955).

[8]R. Loudon, Adv. Phys. 13, 423 (1964).

[9]R. M. Moon, Phys. Rev. Lett. 25, 527 (1970); J. Appl. Phys. 14, 883 (1970).

[10]C. J. Bradley and A. P. Cracknell, *The Mathematical Theory of Symmetry in Solids* (Clarendon, Oxford, 1972).

[11]P. A. Fleury and R. Loudon, Phys. Rev. 166, 514 (1968).

[12]A. P. Cracknell, J. Phys. C 2, 500 (1969).